Carbon 143 (2019) 762–768

Contents lists available at ScienceDirect

Carbon

journal homepage: www.elsevier.com/locate/carbon

Modifying the electrical properties of graphene by reversible point-ripple formation

Mona M.M. Alyobi [a, c], Chris J. Barnett [a], Paul Rees [a], Richard J. Cobley [a, b, *]

[a] College of Engineering, Swansea University, Bay Campus, Swansea, SA1 8EN, United Kingdom
[b] Centre for Nanohealth, Swansea University, Singleton Park, Swansea, SA2 8PP, United Kingdom
[c] College of Science, Taibah University, Universities Road, Medina PO Box: 344, Saudi Arabia

ARTICLE INFO

Article history:
Received 22 September 2018
Received in revised form
12 November 2018
Accepted 26 November 2018
Available online 27 November 2018

ABSTRACT

Strain, ripples and wrinkles in graphene reduce the charge-carrier mobility and alter the electronic behaviour. In few-layer graphene the anisotropy between the in-plane and cross-plane resistivity is altered and a band gap can be opened up. Here we demonstrate a method to reversibly induce point ripples in electrically isolated few-layer graphene with the ability to select the number of layers used for transport measurement down to single layer. During ripple formation the in-plane and cross-plane sheet resistances increase by up to 78% and 699% respectively, confirming that microscopic corrugation changes can solely account for graphene's non-ideal charge-carrier mobility. The method can also count the number of layers in few-layer graphene and is complimentary to Raman spectroscopy and atomic force microscopy when $n \leq 4$. Understanding these changes is crucial to realising practical oscillators, nano-electromechanical systems and flexible electronics with graphene.

1. Introduction

Graphene's excellent electronic, optical and mechanical properties make it an ideal candidate for flexible electronics, sensors and opto-electronics [1,2]. However, strain, ripples and wrinkles in graphene reduce charge transport, can open up a band gap and increase contact resistance [1,3–5]. Ripples could also be the dominant form of scattering in graphene, leading to measured charge mobilities much lower than theoretically predicted [4,6]. As a strong, thin and flexible material graphene is well suited for integration in to oscillating nano-electromechanical systems (NEMS). Yet strain and ripples can alter the flexural modes of graphene, or the induced vibrations can themselves lead to strain which then alters the material properties [4,7]. Understanding how strain and deformation in 2D materials alters the electronic transport is critical to integrating them in to devices [3,4].

Few-layer graphene is less affected by substrate and impurity effects and can mitigate some of these detrimental strain effects [8,9]. To understand the effects of strain on graphene transport it is essential to decouple the in-plane and cross-plane contributions to charge transport. However most studies of conductivity changes in few-layer graphene repeatedly deposit single or bi-layer graphene measuring the change in total conductivity of the stack, leading to orientation mis-match, mechanical damage and contamination [10–16]. The lithographic formation of contacts can also contaminate the sample [17,18].

Direct probe contact to nano-materials instead provides a local, non-destructive and comparably fast technique for electronic transport measurements [19–22]. Here we use a multi-probe method with local probe electrostatic manipulation to controllably and reproducibly perturb mechanically exfoliated few-layer graphene creating a localized ripple or wrinkle in the layers while simultaneously measuring resistance. As the probe is retracted, all sheets are initially pulled with the probe via electrostatic attraction until restoring mechanical forces cause each sheet to detach one at a time from the probe. Discrete drops in tunnelling current are observed as each sheet detaches, just like flipping through a deck of playing cards. With precise control over the process we reverse and repeat the nano-scale manipulation, controllably and reversibly inducing and removing strain in few-layer graphene. By fitting the experimentally-observed current response to a network model we measure in-plane sheet resistance increases of 78% and out of plane increases of 699% due solely to the locally-induced ripple in the graphene. Releasing the ripple

* Corresponding author. College of Engineering, Swansea University, Bay Campus, Swansea, SA1 8EN, United Kingdom.
E-mail address: richard.j.cobley@swansea.ac.uk (R.J. Cobley).

https://doi.org/10.1016/j.carbon.2018.11.076

restores the original conductivities, and by clustering the observed current steps we are also able to count the number of graphene layers. Performed within an ultra-high vacuum chamber, conductivity changes arise solely from the induced strain, confirming that such localized ripples in graphene can alone account for measured conductivity reductions, and offer a way to directly study the transport changes in graphene when used in flexible electronics and NEMS.

2. Experimental

Graphene samples were prepared by mechanical exfoliation of highly-oriented pyrolytic graphite on to the surface of a 90 nm SiO_2 layer on Si grown by thermal oxidation and calibrated by ellipsometry. Flakes containing few-layer graphene were identified initially by scanning electron microscopy (SEM) and then confirmed by Raman spectroscopy and atomic force microscopy (AFM).

Samples were annealed at 200 °C for an hour in ultra-high vacuum (UHV), within an Omicron multi-probe system [23]. In the analysis chamber two tips were approached under SEM guidance to contact the sample for measurement at room temperature as described in the caption of Fig. 1. Tips were electrochemically etched from tungsten and annealed in the UHV chamber to remove surface oxide [24].

While most STM investigations use a feedback-on approach and change the tunnelling conditions [25–28], the resulting tip displacements couple the change in tunnelling set point height with the tip movement that accounts for graphene height changes. Here instead we employ the less-used feedback-off method, where the tip height is controlled, voltage is fixed for each set of measurements, and the resulting tunnelling current change is measured when the probe moves up and down in z only without x or y displacement. Using standard notation these are classified as feedback-off I(z) measurements with a fixed voltage V, where I is the tunnelling current and z the out-of-plane displacement of the probe. Pristine highly oriented graphene is mechanically exfoliated on to the technologically-relevant insulating substrate SiO_2 and annealed in UHV to remove contaminants. No further processing steps or contact fabrication is required. The graphene deflects out of plane remaining in contact with the tip, such that its deflection away from the initial contact point is expected to be equal to the tip z displacement. The lateral extension of the graphene manipulation is however unknown, making quantitative determinations of the locally-induced strain or loading not possible.

The incremental current drop behaviour was observed more than one hundred times on this sample, where the probe voltage was held constant and a script automatically approached and retracted the tip at constant speed to collect I(z) data. The repeated results for each voltage form a single data set which are clustered and fitted as described to extract circuit parameters.

The fits presented in the few-layer section to all six layers of graphene are a single fit, with a second example given in supplementary data for comparison (see Appendix A). To confirm this

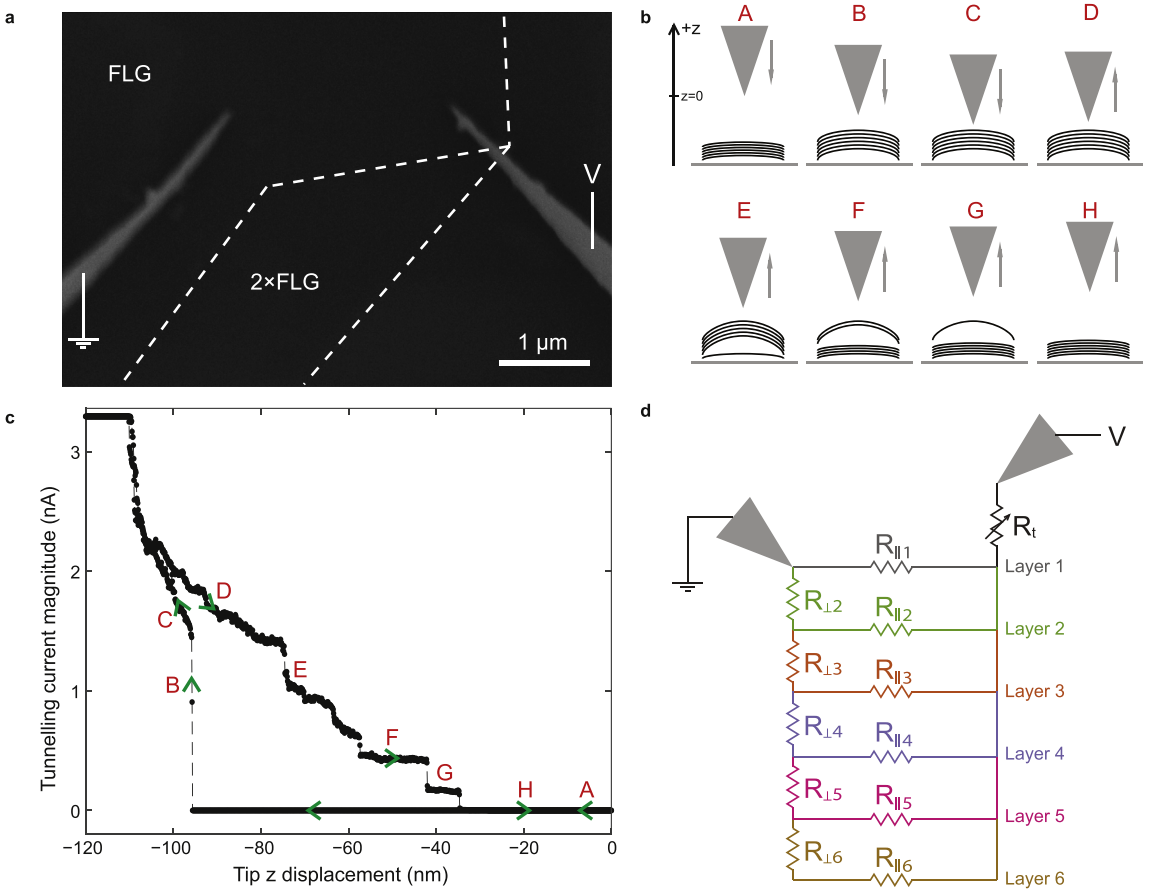

Fig. 1. Transport measurements of few-layer graphene. (a) *In situ* SEM image of probes on few-layer graphene; left probe in contact at ground, right probe biased and movable. Dashed white lines indicate the edges of the few-layer graphene. (b) Schematic of the different stages of probe-graphene interaction during biased right probe approach and withdraw. (c) Example approach-retraction current measurement for tip bias −0.1 V with matching labels. (d) The ladder network model used to fit the retraction data. (A colour version of this figure can be viewed online.)

behaviour was not a localized effect this sample was tested at other locations on the flake, and the method was applied a similar number of times on a second thicker few-layer graphene sample. The results have been re-created with two other tips which all displayed similar behaviour. The results presented here are all taken sequentially at the same location with no lateral movement of the STM tip between the start and finish of the experiment.

3. Results and discussion

3.1. Single- and bi-layer behaviour

Fig. 1a shows two STM probes positioned over a flake of few-layer graphene on a SiO_2 substrate. To aid the eye the dashed white lines show the edge of the flake within the image, with the bottom right of the flake folded back over on itself. The left probe is in direct mechanical contact with the graphene and held at ground in order to provide a constant resistance path back out of the graphene, which is included in the model [29]. The right probe is biased to ±0.1 V, ±0.2 V and ±0.5 V, and moved towards and away from the graphene in the z-direction perpendicular to the graphene layer at a constant speed ten times for every voltage. The schematic in Fig. 1b shows the interaction regimes which occur during probe movement, with the same labels used on an example current measurement in Fig. 1c.

Initially (A) the tip is out of contact with the graphene, and starting from $z = 0$ moves towards the graphene (z becoming negative). The measured tunnelling current is zero until at point B the electrostatic field of the probe causes the graphene stack to deflect up towards the probe with a near-discontinuous increase in measured current. STM of graphene is known to create a local ripple as the sheet or sheets 'jump' to tunnelling contact with the tip [25,30]. Our measured current of ~1.5 nA confirms the probe is not in intimate contact with the graphene stack, with a tunnelling distance still present. In regime C the probe continues to move towards the now deflected graphene stack with an exponential increase in the tunnelling current, indicative of reducing the tunnelling gap between the tip and the graphene. No further discontinuous increases in current are observed indicating that all sheets in the few-layer graphene stack have been perturbed upwards towards the probe and are participating in the conduction network. At 3.3 nA the current pre-amplifier reaches its limit and the automatic routine reverses direction and begins retracting the probe. The probe then retraces a different exponential curve in regime D, discussed later, and via the electrostatic attraction is able to stretch or buckle the graphene from the height at which it jumped to the probe (point B) by around 20 nm, before at point E the restoring elastic forces cause the bottom layer of the stack to detach. This gives rise to a smaller discontinuous current drop, and as the probe continues to retract a series of further discontinuous current drops are evident as the remaining layers detach leaving bi-layer graphene in F and single layer graphene in G. By regime H, all layers have either unbuckled or detached from the probe and the tunnelling current returns to zero.

Data presented here all use the same approach and retraction speed and displacement to keep these mechanics constants. We ensure the tip and graphene do not go in to intimate contact by checking at the lowest voltage setting that maximum current does not saturate the pre-amplifier. We are able to stop the movement of the tip at any point in the behaviour and hold that current, including stopping at $n = 2$ and $n = 1$ and thus select the number of layers of graphene used for measurement.

Resistance ladder network models are predominantly used to represent the equivalent circuit for multi-layer graphene transport [11,31,32]. Using a single contact point model where parameters vary with tip height z, an equivalent circuit for the system is constructed shown in Fig. 1d where $R_{||}$ is the in-plane resistance, $R_{\perp}$ the cross-plane resistance and R_t the tunnelling or access resistance of the probe to the graphene. The model finds that for $R_{||} \gg R_{\perp}$ the last two steps corresponding to bi-layer and single layer graphene are roughly equally spaced and less likely to vary in current magnitude during tip retraction, matching the experimental observation in Fig. 1c. Note that the cross-plane resistance is measured over the interlayer spacing of graphene; a path length considerably shorter than the lateral probe spacing over which the in-plane resistance is measured. Therefore although the cross-plane resistance is lower, when adjusted for path length as sheet resistances or resistivity the expected result that the cross-plane component is much higher is observed.

The clear presentation of the final two steps allowed a custom step detection clustering algorithm to detect and cluster them in all voltage data sets, and fit the current characteristics of each probe voltage data set to the model. Two example data sets for ±0.5 V are shown in Fig. 2a and b, with the fits for all voltages overlaid in Fig. 2c. To make the results comparable with other work [11–13,31,33,34], the fitted tunnelling resistance dependence is removed and the resulting fit is the network model presented earlier with R_t subtracted. For each voltage the set of ten I(z) traces is simultaneously fitted to the model as a non-linear least squares problem to produce the component network values shown for all six voltages.

Graphene is known to conform to the surface roughness of SiO_2 increasing the adhesion and allowing strain engineering [35]. We have previously shown that annealing increases the conformation to such an extent that few layer graphene can become 'invisible' on SiO_2 via electron microscopy [23]. It is likely that this inherent adhesion is providing competing substrate forces which act in the opposite direction to the applied tip forces which, when combined with the elasticity of graphene, define the extension at which each buckled graphene sheet will detach from the tip and return to its rest position. The minimal overlap in the z-direction of each cluster indicates that this process is stable and repeatable.

As expected the total resistance of the graphene stack decreases with increasing layer number – the lower total resistance of few-layer graphene may be preferable for device integration over single layer graphene [10,14,36]. As the tip retracts within each step the tip-graphene distance increases slightly leading to increased tunnelling resistance and lower current, observed as the gradient in the data and fit. Converting to equivalent sheet resistances the mean values of all the in-plane resistances $R_{||}$ corresponding to the values shown in Fig. 2 are then measured to be 10.8 kΩ/sq for both individual sheets in bi-layer graphene, increasing to 13.2 kΩ/sq for single layer. These are higher than those typically reported, which will be addressed shortly.

The weak van der Waals interlayer coupling of graphene sheets always gives rise to higher cross plane resistivity, reported between two and seven orders of magnitude higher than in-plane [33,37]. Converting to sheet resistances, we find here that the mean out-of-plane resistance $R_{\perp}$ for all six voltages is 1505 times higher than $R_{||}$ for bi-layer graphene. These data are addressed together later.

3.2. Few-layer graphene behaviour

This method can also be used to identify the number of graphene layers by counting the incremental current steps as each layer detaches. Multiple sheets can sometimes detach together giving larger but fewer current drops, so to see the general behaviour it is necessary to look at several traces together. Fig. 3 shows twelve multiple repeats at −0.1 V overlaid, which is representative of observed behaviour at other probe voltages. The final

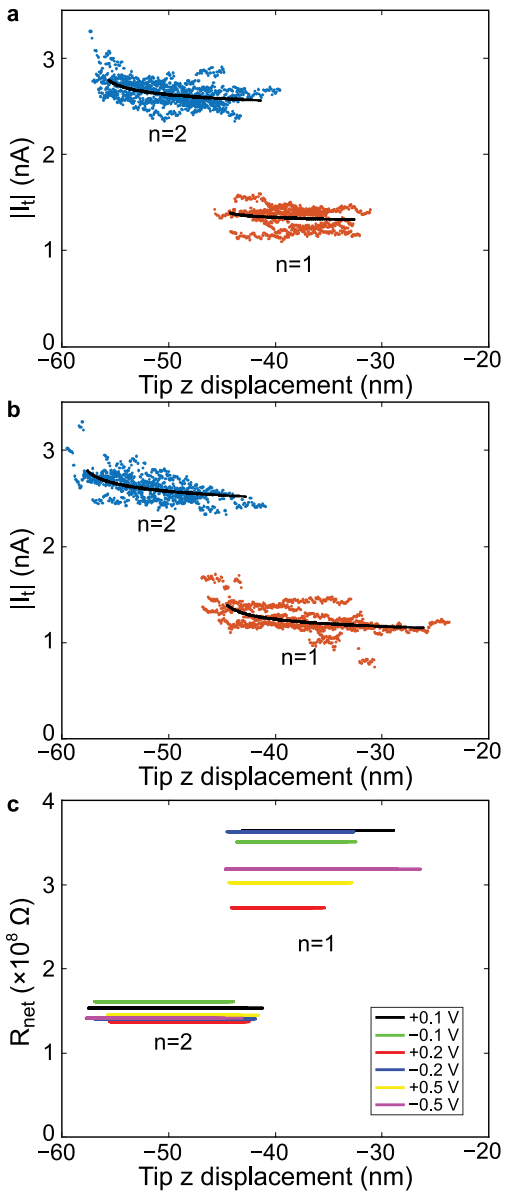

Fig. 2. Automatic step detection of multiple retraction measurements. A clustering algorithm identifies the final two steps corresponding to the measurement of bi-layer and single layer graphene which is then fitted to the network model to find component resistances of the graphene sheets. Shown here are two examples for tip bias (a) +0.5 V and (b) −0.5 V. (c) the fits for six data sets are overlaid showing the total network resistance without the tunnelling resistance R_t. (A colour version of this figure can be viewed online.)

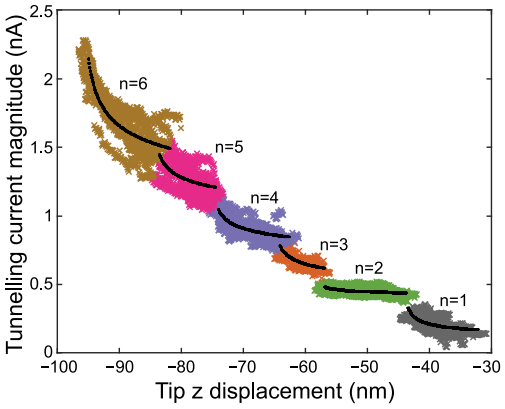

Fig. 3. Twelve overlaid retraction data sets for probe bias −0.1 V, with clustering identifying the steps corresponding to the six layers of graphene. Data corresponding to n = 1 and n = 2 are clustered automatically, then fitted to the network model to generate predicted bounds for the next step, which informs manual selection of the points. Selected points are assigned to the next step, the fit is updated and the process iterates until complete, indicating here six layers of graphene. Black lines indicate the fit of the network model to the data. (A colour version of this figure can be viewed online.)

two steps corresponding to bi-layer and single layer graphene are again clearly evident and can be detected by our combined step-finding clustering algorithm. In this example the next two clusters corresponding to n = 3 and n = 4 are evident by eye, but here we develop a semi-autonomous method to count the higher layer numbers where it becomes increasingly difficult to automatically detect the clusters. To avoid a subjective assessment we first detect the final two steps for n = 2 and n = 1 automatically, and then use the model to predict the likely extrema of the step corresponding to n = 3. This identifies a cluster which is manually selected to represent n = 3. The model then updates the fit to the last three layers and estimates the extrema for step n = 4. The points for this cluster are manually selected and this process is repeated until all steps are accounted for. Using this method we are able to count six layers of graphene which matches individual traces where clear separation of all steps are observed.

While STM has been used directly to determine the thickness of graphene sheets through the topographic height changes [38,39] or through the changes in tunnelling spectroscopy [38,40] the methods are usually limited to very few-layers and require calibration against known samples or another technique. Atomic force microscopy can also be used to estimate the number of layers in graphene, but these measurements suffer from an experimental offset which can be greater than the height of a single sheet, results differ in vacuum and air, and are affected by surface contamination including absorbed water [41–43]. Raman spectroscopy has been used effectively to identify single-layer graphene but sometimes competing analysis methods report different thicknesses when differentiating between bi-layer and other few-layer graphene [44,45]. The electrostatic manipulation method used here can clearly and automatically determine whether a sample is bi-layer or single layer, and by fitting to a network model can accurately determine few-layer graphene layer numbers.

To compare our measurement of the number of layers, we performed Raman spectroscopy where the ratio of the 2D to G peaks and 2D position indicated the sheet consists of around 5 to 6 layers. We also performed ambient contact mode AFM where a height measurement indicated between 5 and 7 layers. As these are in agreement we believe our measurement of six layers to be correct. There is some ambiguity when the layers numbers go above 4, but for n ≤ 4 our method is complimentary to Raman and AFM for counting the number of layers in graphene.

The results of the fit to all six layers also allow a re-examination of the network parameters now for all six steps. Table 1 shows the equivalent in-plane and cross-plane sheet resistances of each individual sheet in the graphene. More information on the conversion is given in the Supplementary Data File - section 4 (see Appendix A). When the probe initially picks up the graphene stack with all six layers (n = 6) the equivalent sheet resistance of each layer separately is measured to be 6.5 kΩ/sq, but as the stack is stretched the sheet resistance increases up to 78% of the initial measurement. This sheet resistance change is not due to the number of layers changing; the model decouples the equivalent sheet resistance for a single sheet of graphene instead of the lumped total network resistance. Similarly when the probe picks up all

Table 1
Equivalent in-plane and out-of-plane sheet resistances of each individual sheet in graphene with n layers, with the percentage increase as the graphene is stretched by the retracting probe biased at −0.1 V.

n	$R_{\|\|}$		$R_{\perp}$		$R_{\perp}/R_{\|\|}$
	kΩ/sq	% change	kΩ/sq	% change	
6	6.5	0	2806	0	434
5	7.2	11	6510	132	904
4	8.6	32	10040	258	1168
3	10.1	55	14858	429	1470
2	11.4	75	22427	699	1969
1	11.6	78			

six layers the cross-plane equivalent sheet resistance for each layer separately is measured to be 2806 kΩ/sq increasing to almost seven times this by the time the graphene has been stretched far enough for all but two sheets to decouple from the probe.

Reported in-plane sheet resistances for single layers of graphene are typically in the range 0.1–2.7 kΩ/sq [11–13,31,33,34]. Here, our results indicate that the initial upwards deformation of the graphene stack to meet the tip induces a ripple which increases the sheet resistance beyond that normally measured on flat graphene. Importantly though, the ripple can be increased by retracting the probe and stretching the graphene, causing a further increase in the measured in-plane sheet resistance.

The values reported earlier for the fit to the last two steps for all voltages are in general agreement with those now derived from a fit to all traces for a single voltage. Both are the same order of magnitude and show increasing in-plane resistance as the stack is stretched and the layer number reduces, most likely due to the formation of long-range scattering potentials as predicted [46–48]. This effect is reversible, with the initial measured resistance matching after each repeat. The height at which the graphene initially deflects up shows a slight drift upwards for the first few measurements at any new position indicating some non-reversible manipulation of the graphene upwards from the substrate. After this there is no further non-reversible movement of the ripple – it recovers to its initial position after every full extension.

By fabricating our few-layer samples from HOPG and separating by electrostatic manipulation we mitigate inter-layer contamination and mis-alignment. This would lead to lower out-of-plane resistance measurements for our study, however this is reversed by the electrostatic manipulation which increases the inter-layer separation and further increases the out-of-plane resistance. The advantage of our study is that we know this out-of-plane resistance increase results from electrostatic manipulation of the graphene and cannot be due to inter-layer contamination. This further demonstrates that impurity-induced scattering is unlikely to be the cause of resistivity changes in graphene since we do not have any inter-layer impurities and yet we are able to modify the in-plane transport properties via ripple formation and extension.

To reduce contamination of the top layer of graphene we anneal samples in UHV and confirm sample quality with Raman. Our direct contact method removes or reduces contamination associated with lithographically formed contacts [49]. Even if some top-layer contamination was present it would simply add an extra access resistance term to the top sheet that would be lumped with, and accounted for, by the tunnelling resistance R_t.

After forming the local ripple in graphene the probe continues to approach tracing an exponential increase in current with distance. However as the probe retracts a different exponential dependence is observed, as shown in Fig. 1c sections C and D. This is different to an observation where compression and release by a contact STM tip on bi-layer graphene traced the same exponential dependence in and out [33]. Our model agrees that the cause of compression-based change is interlayer conductivity, but here we show it is also possible to increase the layer separation to further reduce the cross-plane conductivity. Since our exponential curve is tracing over a different regime on retraction this can only be explained by graphene mechanically responding differently when being pushed by the field, as opposed to being pulled by it.

A similar in-plane resistance increase of around 60% for graphene strained up to 20% has been reported, however this was attributed to “reduced electrical percolation pathways” – a reduction in the number of contact points between graphene layers leading to what is termed here as increased cross plane resistance [50]. Although the method of pre-straining the graphene on a patterned substrate is different to our local electrostatic perturbation method, we have shown that resistance changes of this magnitude can also be achieved by in-plane sheet resistance increases.

Similar STM potentiometry measurements on multi-walled carbon nanotubes (MWCNTs) can be used to estimate the equivalent in-shell and cross-shell conductivity, which are directly comparable to the two directions in graphene measured here [51]. The equivalent cross-plane resistance in MWCNTs is usually higher than graphene as the π-orbital overlap reduces. It has been assumed that beyond three shells there is very little change in the total resistance of MWCNTs. Our method presented here only modifies the sheets directly out-of-plane but it could be possible via multi-probe manipulation to also pull sheets laterally, altering the π-orbital overlap, while still measuring the change in the cross-plane conductivity.

4. Conclusion

We have demonstrated that electrostatic manipulation can be used to repeatedly separate out layers of few-layer graphene, and measure the change in transport as local point ripples are formed and stretched. These increasing resistances resulting from microscopic corrugations are large enough to account for reported low charge carrier mobility in graphene. As they occur here without any change in doping inside an ultra high vacuum chamber they add further weight to the cause of low charge carrier mobility in graphene resulting from disorder-induced scattering potentials rather than dopant-induced changes.

The method can be extended to study other rippling effects including mechanical properties, the formation of electron-hole puddles and the formation of a band gap [52–54]. Controlled rippling in graphene could also lead to spin-based devices [55], and all-graphene strain based devices [54]. Changes in the in-plane and cross-plane anisotropy could lead to mechanically-gated graphene devices [33].

The method can also separate out and count the number of layers of few-layer graphene. In practical few-layer graphene devices the electrical [56], mechanical [57] and thermal [58] properties of the graphene are dependent on the number of layers and this method provides an alternative way to determine the number of layers in few-layer graphene.

Strain can alter the flexural modes of graphene, or when vibrating the induced strain can alter the material properties. Here we demonstrate a way to controllably strain graphene and study directly the change in transport properties, offering a way to study the same effects that occur when graphene is integrated in to NEMS.

Acknowledgements

MMA thanks a Saudi Scholarship (Taibah University, Kingdom of

Saudi Arabia) for financial support. This work was part funded by the Engineering and Physical Sciences Research Council U.K., grant number EP/N013506/1. We thank Professor Richard Palmer for advice in preparing the manuscript.

Appendix A. Supplementary data

Supplementary data to this article can be found online at https://doi.org/10.1016/j.carbon.2018.11.076.

References

[1] B. Vasić, A. Zurutuza, R. Gajić, Spatial variation of wear and electrical properties across wrinkles in chemical vapour deposition graphene, Carbon 102 (2016) 304–310.
[2] X. Li, T. Yang, Y. Yang, J. Zhu, L. Li, F.E. Alam, et al., Large-Area ultrathin graphene films by single-step marangoni self-assembly for highly sensitive strain sensing application, Adv. Funct. Mater. 26 (9) (2016) 1322–1329.
[3] F. Guan, X. Du, Random gauge field scattering in monolayer graphene, Nano Lett. 17 (11) (2017) 7009–7014.
[4] G.G. Naumis, S. Barraza-Lopez, M. Oliva-Leyva, H. Terrones, Electronic and optical properties of strained graphene and other strained 2D materials: a review, Rep. Prog. Phys. 80 (9) (2017).
[5] P. Bøggild, D.M. Mackenzie, P.R. Whelan, D.H. Petersen, J.D. Buron, A. Zurutuza, et al., Mapping the electrical properties of large-area graphene, 2D Mater. 4 (4) (2017) 042003.
[6] N.J. Couto, D. Costanzo, S. Engels, D.-K. Ki, K. Watanabe, T. Taniguchi, et al., Random strain fluctuations as dominant disorder source for high-quality on-substrate graphene devices, Phys. Rev. X 4 (4) (2014) 041019.
[7] B. Amorim, A. Cortijo, F. de Juan, A. Grushin, F. Guinea, A. Gutiérrez-Rubio, et al., Novel effects of strains in graphene and other two dimensional materials, Phys. Rep. 617 (2016) 1–54.
[8] Y. Sui, J. Appenzeller, Screening and interlayer coupling in multilayer graphene field-effect transistors, Nano Lett. 9 (8) (2009) 2973–2977.
[9] Y. Ni, Y. Chalopin, S. Volz, Significant thickness dependence of the thermal resistance between few-layer graphenes, Appl. Phys. Lett. 103 (6) (2013) 061906.
[10] X. Li, Y. Zhu, W. Cai, M. Borysiak, B. Han, D. Chen, et al., Transfer of large-area graphene films for high-performance transparent conductive electrodes, Nano Lett. 9 (12) (2009) 4359–4363.
[11] A. Kasry, M.A. Kuroda, G.J. Martyna, G.S. Tulevski, A.A. Bol, Chemical doping of large-area stacked graphene films for use as transparent, conducting electrodes, ACS Nano 4 (7) (2010) 3839–3844.
[12] S. Bae, H. Kim, Y. Lee, X. Xu, J.-S. Park, Y. Zheng, et al., Roll-to-roll production of 30-inch graphene films for transparent electrodes, Nat. Nanotechnol. 5 (8) (2010) 574–578.
[13] S. Lee, K. Lee, C.-H. Liu, Z. Zhong, Homogeneous bilayer graphene film based flexible transparent conductor, Nanoscale 4 (2) (2012) 639–644.
[14] K.R. Paton, E. Varrla, C. Backes, R.J. Smith, U. Khan, A. O'Neill, et al., Scalable production of large quantities of defect-free few-layer graphene by shear exfoliation in liquids, Nat. Mater. 13 (6) (2014) 624–630.
[15] S. Latil, L. Henrard, Charge carriers in few-layer graphene films, Phys. Rev. Lett. 97 (3) (2006) 036803.
[16] H. Min, P. Jain, S. Adam, M.D. Stiles, Semiclassical Boltzmann transport theory for graphene multilayers, Phys. Rev. B 83 (19) (2011) 195117.
[17] M. Ishigami, J.H. Chen, W.G. Cullen, M.S. Fuhrer, E.D. Williams, Atomic structure of graphene on SiO2, Nano Lett. 7 (6) (2007) 1643–1648.
[18] J. Arnhild, M.K. Fabian, J.S. Wendelin, E. Klaus, Towards electron transport measurements in chemically modified graphene: effect of a solvent, New J. Phys. 12 (12) (2010) 125007.
[19] M.B. Klarskov, H.F. Dam, D.H. Petersen, T.M. Hansen, A. Löwenborg, T. Booth, et al., Fast and direct measurements of the electrical properties of graphene using micro four-point probes, Nanotechnology 22 (44) (2011) 445702.
[20] C.J. Barnett, N.A. Smith, D.R. Jones, T.G. Maffeis, R.J. Cobley, Effects of vacuum annealing on the conduction characteristics of ZnO nanosheets, Nanoscale Res. Lett. 10 (1) (2015) 1.
[21] A.M. Lord, T.G. Maffeis, O. Kryvchenkova, R.J. Cobley, K. Kalna, D.M. Kepaptsoglou, et al., Controlling the electrical transport properties of nanocontacts to nanowires, Nano Lett. 15 (7) (2015) 4248–4254.
[22] C.J. Barnett, O. Kryvchenkova, N.A. Smith, L. Kelleher, T.G. Maffeis, R.J. Cobley, The effects of surface stripping ZnO nanorods with argon bombardment, Nanotechnology 26 (41) (2015) 415701.
[23] M. Alyobi, C. Barnett, R. Cobley, Effects of thermal annealing on the properties of mechanically exfoliated suspended and on-substrate few-layer graphene, Crystals 7 (11) (2017) 349.
[24] R.J. Cobley, R.A. Brown, C.J. Barnett, T.G.G. Maffeis, M.W. Penny, Quantitative analysis of annealed scanning probe tips using energy dispersive x-ray spectroscopy, Appl. Phys. Lett. 102 (2) (2013).
[25] F.R. Eder, J. Kotakoski, K. Holzweber, C. Mangler, V. Skakalova, J.C. Meyer, Probing from both sides: reshaping the graphene landscape via face-to-face dual-probe microscopy, Nano Lett. 13 (5) (2013) 1934–1940.
[26] R. Breitwieser, Y.-C. Hu, Y.C. Chao, R.-J. Li, Y.R. Tzeng, L.-J. Li, et al., Flipping nanoscale ripples of free-standing graphene using a scanning tunneling microscope tip, Carbon 77 (2014) 236–243.
[27] P. Xu, M. Neek-Amal, S. Barber, J. Schoelz, M. Ackerman, P. Thibado, et al., Unusual ultra-low-frequency fluctuations in freestanding graphene, Nat. Commun. 5 (2014).
[28] M. Neek-Amal, P. Xu, J. Schoelz, M. Ackerman, S. Barber, P. Thibado, et al., Thermal mirror buckling in freestanding graphene locally controlled by scanning tunnelling microscopy, Nat. Commun. 5 (2014).
[29] N.A. Smith, A.M. Lord, J.E. Evans, C.J. Barnett, R.J. Cobley, S. Wilks, Forming reproducible non-lithographic nanocontacts to assess the effect of contact compressive strain in nanomaterials, Semicond. Sci. Technol. 30 (6) (2015) 065011.
[30] N.N. Klimov, S. Jung, S. Zhu, T. Li, C.A. Wright, S.D. Solares, et al., Electromechanical properties of graphene drumheads, Science 336 (6088) (2012) 1557–1561.
[31] K. Ito, M. Katagiri, T. Sakai, Y. Awano, Electrical resistivity measurements of layer number determined multilayer graphene wiring for future large scale integrated circuit interconnects, Jpn. J. Appl. Phys. 52 (6S) (2013) 06GD8.
[32] Modeling and optimization for multi-layer graphene nanoribbon conductors, in: V. Kumar, S. Rakheja, A. Naeemi (Eds.), Interconnect Technology Conference and 2011 Materials for Advanced Metallization (IITC/MAM), 2011 IEEE International, IEEE, 2011.
[33] P.W. Sutter, J.-I. Flege, E.A. Sutter, Epitaxial graphene on ruthenium, Nat. Mater. 7 (5) (2008) 406–411.
[34] I. Khrapach, F. Withers, T.H. Bointon, D.K. Polyushkin, W.L. Barnes, S. Russo, et al., Novel highly conductive and transparent graphene-based conductors, Adv. Mater. 24 (21) (2012) 2844–2849.
[35] W.G. Cullen, M. Yamamoto, K.M. Burson, J.H. Chen, C. Jang, L. Li, et al., High-fidelity conformation of graphene to ${\mathrm{SiO}}_{2}$ topographic features, Phys. Rev. Lett. 105 (21) (2010) 215504.
[36] M. Kaempgen, G. Duesberg, S. Roth, Transparent carbon nanotube coatings, Appl. Surf. Sci. 252 (2) (2005) 425–429.
[37] D.Z. Tsang, M.S. Dresselhaus, C-axis electrical-conductivity of kish graphite, Carbon 14 (1) (1976) 43–46.
[38] V.W. Brar, Y. Zhang, Y. Yayon, T. Ohta, J.L. McChesney, A. Bostwick, et al., Scanning tunneling spectroscopy of inhomogeneous electronic structure in monolayer and bilayer graphene on SiC, Appl. Phys. Lett. 91 (12) (2007) 122102.
[39] A. Luican, G. Li, E.Y. Andrei, Scanning tunneling microscopy and spectroscopy of graphene layers on graphite, Solid State Commun. 149 (27–28) (2009) 1151–1156.
[40] P. Lauffer, K. Emtsev, R. Graupner, T. Seyller, L. Ley, S. Reshanov, et al., Atomic and electronic structure of few-layer graphene on SiC (0001) studied with scanning tunneling microscopy and spectroscopy, Phys. Rev. B 77 (15) (2008) 155426.
[41] Z. Ni, Y. Wang, T. Yu, Z. Shen, Raman spectroscopy and imaging of graphene, Nano Res. 1 (4) (2008) 273–291.
[42] Y.K. Koh, M.-H. Bae, D.G. Cahill, E. Pop, Reliably counting atomic planes of few-layer graphene (n> 4), ACS Nano 5 (1) (2010) 269–274.
[43] H. Li, J. Wu, X. Huang, G. Lu, J. Yang, X. Lu, et al., Rapid and reliable thickness identification of two-dimensional nanosheets using optical microscopy, ACS Nano 7 (11) (2013) 10344–10353.
[44] D. Graf, F. Molitor, K. Ensslin, C. Stampfer, A. Jungen, C. Hierold, et al., Spatially resolved Raman spectroscopy of single-and few-layer graphene, Nano Lett. 7 (2) (2007) 238–242.
[45] Y. Hao, Y. Wang, L. Wang, Z. Ni, Z. Wang, R. Wang, et al., Probing layer number and stacking order of few-layer graphene by Raman spectroscopy, Small 6 (2) (2010) 195–200.
[46] M. Katsnelson, A. Geim, Electron scattering on microscopic corrugations in graphene, Phil. Trans. Roy. Soc. Lond.: Math. Phys. Eng. Sci. 366 (1863) (2008) 195–204.
[47] F. Schedin, A. Geim, S. Morozov, E. Hill, P. Blake, M. Katsnelson, et al., Detection of individual gas molecules adsorbed on graphene, Nat. Mater. 6 (9) (2007) 652–655.
[48] K. Xu, P. Cao, J.R. Heath, Scanning tunneling microscopy characterization of the electrical properties of wrinkles in exfoliated graphene monolayers, Nano Lett. 9 (12) (2009) 4446–4451.
[49] M.K. Yakes, D. Gunlycke, J.L. Tedesco, P.M. Campbell, R.L. Myers-Ward, C.R. Eddy, et al., Conductance anisotropy in epitaxial graphene sheets generated by substrate interactions, Nano Lett. 10 (5) (2010) 1559–1562.
[50] Y. Wang, R. Yang, Z. Shi, L. Zhang, D. Shi, E. Wang, et al., Super-elastic graphene ripples for flexible strain sensors, ACS Nano 5 (5) (2011) 3645–3650.
[51] A. Stetter, J. Vancea, C.H. Back, Determination of the intershell conductance in a multiwall carbon nanotube, Appl. Phys. Lett. 93 (17) (2008) 172103.
[52] P. Partovi-Azar, N. Nafari, M.R.R. Tabar, Interplay between geometrical structure and electronic properties in rippled free-standing graphene, Phys. Rev. B 83 (16) (2011).
[53] K.-K. Bai, Y. Zhou, H. Zheng, L. Meng, H. Peng, Z. Liu, et al., Creating one-dimensional nanoscale periodic ripples in a continuous mosaic graphene monolayer, Phys. Rev. Lett. 113 (8) (2014) 086102.
[54] R. Miranda, A.L.V. de Parga, Graphene: surfing ripples towards new devices, Nat. Nanotechnol. 4 (9) (2009) 549–550.
[55] G.X. Ni, Y. Zheng, S. Bae, H.R. Kim, A. Pachoud, Y.S. Kim, et al., Quasi-periodic nanoripples in graphene grown by chemical vapor deposition and its impact

on charge transport, ACS Nano 6 (2) (2012) 1158–1164.
[56] K. Nagashio, T. Nishimura, K. Kita, A. Toriumi, Mobility variations in mono-and multi-layer graphene films, APEX 2 (2) (2009) 025003.
[57] M. Poot, H.S. van der Zant, Nanomechanical properties of few-layer graphene membranes, Appl. Phys. Lett. 92 (6) (2008) 063111.
[58] S. Ghosh, W. Bao, D.L. Nika, S. Subrina, E.P. Pokatilov, C.N. Lau, et al., Dimensional crossover of thermal transport in few-layer graphene, Nat. Mater. 9 (7) (2010) 555–558.